Science

Cite as: E. Maguid *et al.*, *Science*
10.1126/science.aaf3417 (2016).

Photonic spin-controlled multifunctional shared-aperture antenna array

Elhanan Maguid,[1]* Igor Yulevich,[1]* Dekel Veksler,[1]* Vladimir Kleiner,[1] Mark L. Brongersma,[2] Erez Hasman[1]†

[1]Micro and Nanooptics Laboratory, Faculty of Mechanical Engineering, and Russell Berrie Nanotechnology Institute, Technion – Israel Institute of Technology, Haifa 32000, Israel. [2]Geballe Laboratory for Advanced Materials, Stanford University, 476 Lomita Mall, Stanford, CA 94305, USA.

*These authors contributed equally to this work.

†Corresponding author. Email: mehasman@technion.ac.il

The shared-aperture phased antenna array developed in the field of radar applications is a promising approach for increased functionality in photonics. The alliance between the shared-aperture concepts and the geometric phase phenomenon arising from spin-orbit interaction provides a route to implement photonic spin-control multifunctional metasurfaces. We adopt a thinning technique within the shared-aperture synthesis and investigate interleaved sparse nanoantenna matrices and spin-enabled asymmetric harmonic response to achieve helicity-controlled multiple structured wave-fronts such as vortex beams carrying orbital angular momentum. Multiplexed geometric phase profiles are utilized for the simultaneous measurement of spectrum characteristics and polarization state of light, enabling integrated on-chip spectropolarimetric analysis. The shared-aperture metasurface platform opens a pathway to novel types of nanophotonic functionality.

Multifunctional planar systems that can perform a number of concurrent tasks in a shared-aperture were recently introduced in the field of phased array antennas for radar applications. In particular, modern RF sensing, communication and imaging systems based on sparse phased array antennas are able to operate at different frequency bands, polarizations, scanning directions, etc. These capabilities are ascribed to sub-arrays of elementary radiators, sharing a common physical area that constitutes the complete aperture of the phased array (*1*–*4*). The shared-aperture concept can be adopted to realize multifunctional photonic antenna arrays. The recent implementation of metasurfaces, or metamaterials of reduced dimensionality, is of particular relevance as it opens up new opportunities to acquire virtually flat optics. Metasurfaces consist of a dense arrangement of resonant optical antennas on a scale smaller than the wavelength of external stimuli (*5*–*10*). The resonant nature of the light-matter interaction of individual nanoantenna affords substantial control over the local light scattering properties. Specifically, the local phase pickup can be manipulated by tailoring the antenna material, size, shape, and environment – antenna resonance shaping (*11*–*15*), or through the geometric phase concept (*10*, *16*–*20*). The latter concept is an efficient approach for achieving spin-controlled phase modulation, whereas the photon spin is associated with the intrinsic angular momentum of light (*21*). Such a geometric phase metasurface (GPM) transforms an incident circularly polarized light into a beam of opposite helicity, imprinted with a geometric phase $\phi_g(x,y)=2\sigma_{\pm}\theta(x,y)$; where $\sigma_{\pm}=\pm 1$ denotes the polarization helicity (photon spin in $\hbar$ units) of the incident light, and $\theta(x,y)$ is the nanoantenna orientation (*22*). Here, we incorporate the shared-aperture phased antenna array concept and spin-controlled two-dimensional optics based on nanoantennas. By use of the geometric phase mechanism, utilizing the spin-orbit interaction phenomenon, a multifunctional GPM is implemented (Fig. 1).

Photonic GPMs with spatially interleaved phase profiles are designed by the random mixing of optical nanoantenna sub-arrays, where each sub-array provides a different phase function in a spin-dependent manner. This approach utilizes the peculiar ability of random patterns to yield extraordinary information capacity, and polarization helicity control via the geometric phase concept. We realized a high efficiency multifunctional GPM in which the phase and polarization distributions of each wave-front are independently controlled. These GPMs are based on gap-plasmon resonator (GPR) nanoantennas that consist of metal-insulator-metal layers enabling high reflectivity by increasing the coupling between the free-wave and the fundamental resonator mode. Moreover, adjustment of the GPR nanoantenna's dimensions enables the design of high efficiency half-wave plate (*22*, *23*). A diffraction efficiency of ~79% was found for the reflection mode of a single wave-front, which is in good agreement with the theory (*10*, *18*, *19*), and the finite-difference time-domain (FDTD) simulation (fig. S1, D to F) (*22*). Then, to design a metasurface generating multiple spin-dependent wave-fronts carrying orbital angular momentum (OAM), the GPR nanoantennas were randomly distributed into equal interleaved sub-arrays. The nanoantennas of each *j*-th sub-array were oriented according to the relation $2\theta_j(x,y) = k_j x + l_j \varphi$, to obtain momentum redirection $\sigma_\pm k_j$ and topological charge (winding number) $\sigma_\pm l_j$; φ is the azimuthal angle (Fig. 2A). We measured the far-field intensity distribution by illuminating the metasurface with circularly polarized light at a wavelength of 760 nm, and observed 3x2 spin-dependent OAM wave-fronts with the desired topological charges of 0, ±1, ±2 (Fig. 2, B and C), in agreement with FDTD simulation (fig. S2). The corresponding OAMs were verified by measuring the dislocation strength by the interference of the vortex beams with a plane-wave (Fig. 2, D and E). An additional peculiar twist in the field of metasurfaces relies on space-variant polarization manipulation, which may encompass a broader class of wave-front shaping. Interleaved GPM enables obtaining multiple vectorial vortices by coherent superposition of wave-fronts with opposite helicities (fig. S6 and movies S1 and S2) (*22*).

The angular resolution characteristics of the interleaved and segmented GPMs were experimentally examined via far-field measurements. In the segmentation approach increasing the number of wave-fronts, *N*, results in an angular width of $\Delta\Theta \sim \sqrt{N}\cdot\lambda/D$, while for the interleaved GPM it is approximately λ/D for an arbitrary *N*, matching the diffraction-limited angular resolution of the shared-aperture of size *D* at a wavelength λ (Fig. 2, F and G, and figs. S4 and S5). However, the above analysis does not hold the promise to obtain high information capacity for the interleaved approach, as it is also strongly influenced by the noise originated from channels mixing. The signal-to-noise ratio (SNR) determines the available number of bits per channel as $\log_2(1 + SNR)$, and sets the limit N_c for the channel capacity when $SNR = 1$. In order to estimate the impact of an incrementally growing number of wave-fronts on SNR, the far-field intensity distributions were calculated via Fourier transform (*22*). The calculation shows that the SNR scales as $1/N^2$, leading to a channel capacity limit of $N_c \approx 130$ for the interleaved GPM of $D = 50$ μm (Fig. 2I). Moreover, both the calculations and experiments show that the intensity per channel decreases according to $1/N^2$ (Fig. 2H).

Unlike the interleaved GPM the harmonic response (HR) metasurface is not limited by the intensity scaling of $1/N^2$. The HR concept relies on different optimization methods, iterative and analytic, and has been implemented in a variety of realms such as holography, communication, and radar (*24*–*26*). In order to obtain spin-dependent asymmetric harmonic diffraction orders we incorporate the HR and geometric phase concepts. The geometric phase function can be expanded to spin-dependent OAM harmonic orders $A_m \exp\left[im\sigma_\pm\left(kx+\varphi\right)\right]$, where $\sigma_\pm mk$ is the momentum redirection of *m-th* order. The phase function can be optimized to achieve identical intensities $\left|A_m\right|^2 \approx 1/\left(b-a+1\right)$ for selected asymmetric orders $a < m < b$ with maximal optical efficiency. We adopted an optimized analytic solution, namely "triplicator" (*25*), to realize a GPM (Fig. 3, A to C) providing three spin-dependent asymmetric OAM harmonic orders (*22*). The GPM was illuminated with right and left circularly polarized light and the spin-dependent diffraction pattern consisting of multiple OAM harmonic orders of $l_\pm = \sigma_\pm, 2\sigma_\pm, 3\sigma_\pm$ corresponding to m = 1, 2, 3 was observed (Fig. 3, D and E). The diffraction patterns were verified by the spin-dependent FDTD simulation (Fig. 3, F and G) and by calculating Fourier amplitudes (Fig. 3, H and I). The efficiencies of each order were measured to be $\left|A_m\right|^2 \cong 0.21$ with uniformity of ± 0.01, leading to a total efficiency of ~63%, in accordance with the intensity scaling of $1/N$ (Fig. 3J) (*22*). Furthermore, we experimentally confirmed that the HR approach is manifested by diffraction-limited angular resolution of the shared aperture (Fig. 2F, and fig. S7, B and F). In light of the above, the HR concept constitutes an excellent platform to realize a well angular resolved multi-beam possessing negligible noise, thus, able to provide high information capacity, while the interleaving approach suffers from the speckle noise and is hindered by capacity reduction. On the other hand, the latter approach offers high flexibility in multifunctional wave-front generation, whereas with the HR concept, harmonic sequence restricts this flexibility. Moreover, the reported spin-controlled multifunctional metasurfaces based on shared-aperture approaches are studied in terms of information capacity by means of Wigner phase-space distribution to establish a link between the Shannon entropy and the capacity of photonic system (fig. S8) (*22*).

Spectropolarimetry is an application for the simultaneous measurement of the spectrum and polarization state of light, and is widely used to characterize chemical compounds. Implementing spectropolarimetric devices with metasurfaces opens new avenues for on-chip detection. Recently, an on-chip chiroptical spectroscopy (*27*) was presented, measuring the differential absorption between left- and right-circular polarizations; however, this device is unable to provide full polarization analysis. Yet it has been shown that a metasurface allows for the simultaneous determination of the Stokes parameters (i.e., the polarization state of light) (*28*, *29*) without consideration of the spectral analysis.

Here we propose a simple, fast and compact technique based on an interleaved GPM, that can simultaneously characterize the polarization state and spectrum of a wave transmitted through a semitransparent object. The spectropolarimeter metasurface (SPM) is composed of three interleaved linear phase profiles $\phi_g^{(1)} = \sigma_\pm k_x x; \phi_g^{(2)} = \sigma_\pm k_y y; \phi_g^{(3)} = -\sigma_\pm k_y y$ associated with different nanoantenna sub-arrays. When a probe beam with an arbitrary polarization state impinges on the SPM, two beams of intensities $I_{\sigma_\pm}$, consist of opposite helicity states, and two additional beams emerge. The latter have identical polarizations, conjugate with respect to the incident beam, and being projected onto linear polarizers at 0 and 45 degrees determine the linearly polarized components I_{L0} and I_{L45}, respectively (Fig. 4A). The Stokes parameters of the probed beam are then calculated by the following expressions (*28*): $S_0 = 2\left(I_{\sigma_+} + I_{\sigma_-}\right)/\eta; S_1 = 2I_{L0}/\eta - S_0;$ $S_2 = 2I_{L45}/\eta - S_0; S_3 = 2\left(I_{\sigma_+} - I_{\sigma_-}\right)/\eta$, where η is determined by a calibration experiment (fig. S9). The SPM of 50 μm diameter was normally illuminated by a supercontinuum light source, passing through the acousto-optic modulator which enables the tenability of various wavelengths. Figure 4B shows the measured and calculated Stokes parameters on a Poincaré sphere for an analyzed beam impinging the SPM at a wavelength of 760 nm with different polarizations, obtained by a polarization-state generator (linear polarizer followed by a rotated quarter-wave plate). The spectral resolving power is defined according to the Rayleigh criterion as $\lambda/\Delta\lambda = q/M_{x,y}^{\ 2}$, where $M_{x,y}^{\ 2}$ is the beam quality parameter in each direction (x, y), and q is the number of phase modulation periods (*30*). The resolving power of the SPM was measured and found to be $\lambda/\Delta\lambda \cong 13$ (Fig. 4C). The obtained value is in good agreement with the calculated resolving power for SPM with $q \cong 17$ periods, and a laser beam quality of $M_{x,y}^{\ 2} = 1.3$. We measured the optical rotatory dispersion (ORD) for the specific rotations of D-glucose (chiral molecule) and of its enantiomer L-glucose that were dissolved in water with predetermined concentrations (Fig. 4D) (*22*). The ORD of D-glucose shows a good agreement with the values found in the literature (*31*), while the L-glucose ORD manifested the opposite behavior that was expected. To conclude, we achieved real-time on-chip spectropolarimetry by exploiting the interleaved GPM. The reported alliance of the spin-enabled geometric phase and shared-aperture concepts sheds light on the multifunctional wave-front manipulation in a spin-dependent manner. The introduced asymmetric HR and interleaved GPMs constitute excellent candidates to realize on-demand multifunctional on-chip photonics.

REFERENCES AND NOTES

1. D. M. Pozar, S. D. Targonski, A shared-aperture dual-band dual-polarized microstrip array. *IEEE Trans. Antenn. Propag.* **49**, 150–157 (2001). doi:10.1109/8.914255
2. R. L. Haupt, Interleaved thinned linear arrays. *IEEE Trans. Antenn. Propag.* **53**, 2858–2864 (2005). doi:10.1109/TAP.2005.854522
3. A. M. Sayeed, V. Raghavan, Maximizing MIMO capacity in sparse multipath with reconfigurable antenna arrays. *IEEE J. Sel. Top. Signal Process.* **1**, 156–166 (2007). doi:10.1109/JSTSP.2007.897057
4. I. E. Lager, C. Trampuz, M. Simeoni, L. P. Ligthart, Interleaved array antennas for FMCW radar applications. *IEEE Trans. Antenn. Propag.* **57**, 2486–2490 (2009). doi:10.1109/TAP.2009.2024573
5. A. Papakostas, A. Potts, D. M. Bagnall, S. L. Prosvirnin, H. J. Coles, N. I. Zheludev, Optical manifestations of planar chirality. *Phys. Rev. Lett.* **90**, 107404 (2003). Medline doi:10.1103/PhysRevLett.90.107404
6. X. Yin, Z. Ye, J. Rho, Y. Wang, X. Zhang, Photonic spin Hall effect at metasurfaces. *Science* **339**, 1405–1407 (2013). Medline doi:10.1126/science.1231758
7. A. Pors, O. Albrektsen, I. P. Radko, S. I. Bozhevolnyi, Gap plasmon-based metasurfaces for total control of reflected light. *Sci. Rep.* **3**, 2155 (2013). Medline doi:10.1038/srep02155
8. A. V. Kildishev, A. Boltasseva, V. M. Shalaev, Planar photonics with metasurfaces. *Science* **339**, 1232009 (2013). Medline doi:10.1126/science.1232009
9. N. Yu, F. Capasso, Flat optics with designer metasurfaces. *Nat. Mater.* **13**, 139–150 (2014). Medline doi:10.1038/nmat3839
10. D. Lin, P. Fan, E. Hasman, M. L. Brongersma, Dielectric gradient metasurface optical elements. *Science* **345**, 298–302 (2014). Medline doi:10.1126/science.1253213
11. M. G. Nielsen, D. K. Gramotnev, A. Pors, O. Albrektsen, S. I. Bozhevolnyi, Continuous layer gap plasmon resonators. *Opt. Express* **19**, 19310–19322 (2011). Medline doi:10.1364/OE.19.019310
12. D. Dregely, K. Lindfors, M. Lippitz, N. Engheta, M. Totzeck, H. Giessen, Imaging and steering an optical wireless nanoantenna link. *Nat. Commun.* **5**, 4354 (2014). Medline doi:10.1038/ncomms5354
13. J. Sun, X. Wang, T. Xu, Z. A. Kudyshev, A. N. Cartwright, N. M. Litchinitser, Spinning light on the nanoscale. *Nano Lett.* **14**, 2726–2729 (2014). Medline doi:10.1021/nl500658n
14. H.-S. Ee, J.-H. Kang, M. L. Brongersma, M.-K. Seo, Shape-dependent light scattering properties of subwavelength silicon nanoblocks. *Nano Lett.* **15**, 1759–1765 (2015). Medline doi:10.1021/nl504442v
15. K. E. Chong, I. Staude, A. James, J. Dominguez, S. Liu, S. Campione, G. S. Subramania, T. S. Luk, M. Decker, D. N. Neshev, I. Brener, Y. S. Kivshar, Polarization-independent silicon metadevices for efficient optical wavefront control. *Nano Lett.* **15**, 5369–5374 (2015). Medline doi:10.1021/acs.nanolett.5b01752
16. Z. Bomzon, V. Kleiner, E. Hasman, Pancharatnam-Berry phase in space-variant polarization-state manipulations with subwavelength gratings. *Opt. Lett.* **26**, 1424–1426 (2001). Medline doi:10.1364/OL.26.001424
17. Z. Bomzon, G. Biener, V. Kleiner, E. Hasman, Space-variant Pancharatnam-Berry phase optical elements with computer-generated subwavelength gratings. *Opt. Lett.* **27**, 1141–1143 (2002). Medline doi:10.1364/OL.27.001141
18. G. Biener, A. Niv, V. Kleiner, E. Hasman, Formation of helical beams by use of Pancharatnam-Berry phase optical elements. *Opt. Lett.* **27**, 1875–1877 (2002). Medline doi:10.1364/OL.27.001875
19. A. Niv, G. Biener, V. Kleiner, E. Hasman, Manipulation of the Pancharatnam phase in vectorial vortices. *Opt. Express* **14**, 4208–4220 (2006). Medline doi:10.1364/OE.14.004208
20. N. Dahan, Y. Gorodetski, K. Frischwasser, V. Kleiner, E. Hasman, Geometric doppler effect: Spin-split dispersion of thermal radiation. *Phys. Rev. Lett.* **105**, 136402 (2010). Medline doi:10.1103/PhysRevLett.105.136402
21. K. Y. Bliokh, F. J. Rodríguez-Fortuño, F. Nori, A. V. Zayats, Spin–orbit interactions of light. *Nat. Photonics* **9**, 796–808 (2015). doi:10.1038/nphoton.2015.201

22. Full details can be found in the supplementary materials on *Science* Online.
23. A. Pors, M. G. Nielsen, S. I. Bozhevolnyi, Broadband plasmonic half-wave plates in reflection. *Opt. Lett.* **38**, 513–515 (2013). Medline doi:10.1364/OL.38.000513
24. H. Dammann, K. Görtler, High-efficiency in-line multiple imaging by means of multiple phase holograms. *Opt. Commun.* **3**, 312–315 (1971). doi:10.1016/0030-4018(71)90095-2
25. F. Gori, M. Santarsiero, S. Vicalvi, R. Borghi, G. Cincotti, E. Di Fabrizio, M. Gentili, Analytical derivation of the optimum triplicator. *Opt. Commun.* **157**, 13–16 (1998). doi:10.1016/S0030-4018(98)00518-5
26. J. Albero, J. A. Davis, D. M. Cottrell, C. E. Granger, K. R. McCormick, I. Moreno, Generalized diffractive optical elements with asymmetric harmonic response and phase control. *Appl. Opt.* **52**, 3637–3644 (2013). Medline doi:10.1364/AO.52.003637
27. A. Shaltout, J. Liu, A. Kildishev, V. Shalaev, Photonic spin Hall effect in gap–plasmon metasurfaces for on-chip chiroptical spectroscopy. *Optica* **2**, 860–863 (2015). doi:10.1364/OPTICA.2.000860
28. Y. Gorodetski, G. Biener, A. Niv, V. Kleiner, E. Hasman, Space-variant polarization manipulation for far-field polarimetry by use of subwavelength dielectric gratings. *Opt. Lett.* **30**, 2245–2247 (2005). Medline doi:10.1364/OL.30.002245
29. A. Pors, M. G. Nielsen, S. I. Bozhevolnyi, Plasmonic metagratings for simultaneous determination of Stokes parameters. *Optica* **2**, 716–723 (2015). doi:10.1364/OPTICA.2.000716
30. N. Davidson, L. Khaykovich, E. Hasman, High-resolution spectrometry for diffuse light by use of anamorphic concentration. *Opt. Lett.* **24**, 1835–1837 (1999). Medline doi:10.1364/OL.24.001835
31. A. Penzkofer, Optical rotatory dispersion measurement of D-glucose with fixed polarizer analyzer accessory in conventional spectrophotometer. *J. Anal. Sci. Methods Instrum.* **3**, 234–239 (2013).
32. K. Y. Bliokh, M. A. Alonso, E. A. Ostrovskaya, A. Aiello, Angular momenta and spin-orbit interaction of nonparaxial light in free space. *Phys. Rev. A* **82**, 063825 (2010). doi:10.1103/PhysRevA.82.063825
33. N. Shitrit, I. Yulevich, E. Maguid, D. Ozeri, D. Veksler, V. Kleiner, E. Hasman, Spin-optical metamaterial route to spin-controlled photonics. *Science* **340**, 724–726 (2013). Medline doi:10.1126/science.1234892
34. D. Gabor, in *Progress in Optics*, E. Wolf, Ed. (North-Holland, Amsterdam, 1961), vol. 1, pp. 109–153.
35. D. Veksler, E. Maguid, N. Shitrit, D. Ozeri, V. Kleiner, E. Hasman, Multiple wavefront shaping by metasurface based on mixed random antenna groups. *ACS Photonics* **2**, 661–667 (2015). doi:10.1021/acsphotonics.5b00113
36. Y. Yirmiyahu, A. Niv, G. Biener, V. Kleiner, E. Hasman, Vectorial vortex mode transformation for a hollow waveguide using Pancharatnam-Berry phase optical elements. *Opt. Lett.* **31**, 3252–3254 (2006). Medline doi:10.1364/OL.31.003252
37. R. Dorn, S. Quabis, G. Leuchs, Sharper focus for a radially polarized light beam. *Phys. Rev. Lett.* **91**, 233901 (2003). Medline doi:10.1103/PhysRevLett.91.233901
38. V. Shvedov, A. R. Davoyan, C. Hnatovsky, N. Engheta, W. Krolikowski, A long-range polarization-controlled optical tractor beam. *Nat. Photonics* **8**, 846–850 (2014). doi:10.1038/nphoton.2014.242
39. R. Oron, S. Blit, N. Davidson, A. A. Friesem, Z. Bomzon, E. Hasman, The formation of laser beams with pure azimuthal or radial polarization. *Appl. Phys. Lett.* **77**, 3322–3324 (2000). doi:10.1063/1.1327271
40. S. J. Kim, P. Fan, J.-H. Kang, M. L. Brongersma, Creating semiconductor metafilms with designer absorption spectra. *Nat. Commun.* **6**, 7591 (2015). Medline doi:10.1038/ncomms8591
41. M. Hillery, R. F. O'Connell, M. O. Scully, E. P. Wigner, Distribution functions in physics: Fundamentals. *Phys. Rep.* **106**, 121–167 (1984). doi:10.1016/0370-1573(84)90160-1
42. J. M. R. Parrondo, J. M. Horowitz, T. Sagawa, Thermodynamics of information. *Nat. Phys.* **11**, 131–139 (2015). doi:10.1038/nphys3230
43. C. E. Shannon, A mathematical theory of communication. *Bell Syst. Tech. J.* **27**, 379–423 (1948). doi:10.1002/j.1538-7305.1948.tb01338.x
44. T. M. Cover, J. A. Thomas, in *Elements of Information Theory* (Wiley, New Jersey, ed. 2, 2006), chaps. 2, 7.

ACKNOWLEDGMENTS

This research was supported by the United States - Israel Binational Science Foundation (BSF), the Israel Science Foundation, the Israel Nanotechnology Focal Technology Area on Nanophotonics for Detection, and KLA-Tencor.

SUPPLEMENTARY MATERIALS

www.sciencemag.org/cgi/content/full/science.aaf3417/DC1
Supplementary Text
Figures S1 to S9
References (*32*–*44*)
Movies S1 and S2

28 January 2016; accepted 8 April 2016
Published online 21 April 2016
10.1126/science.aaf3417

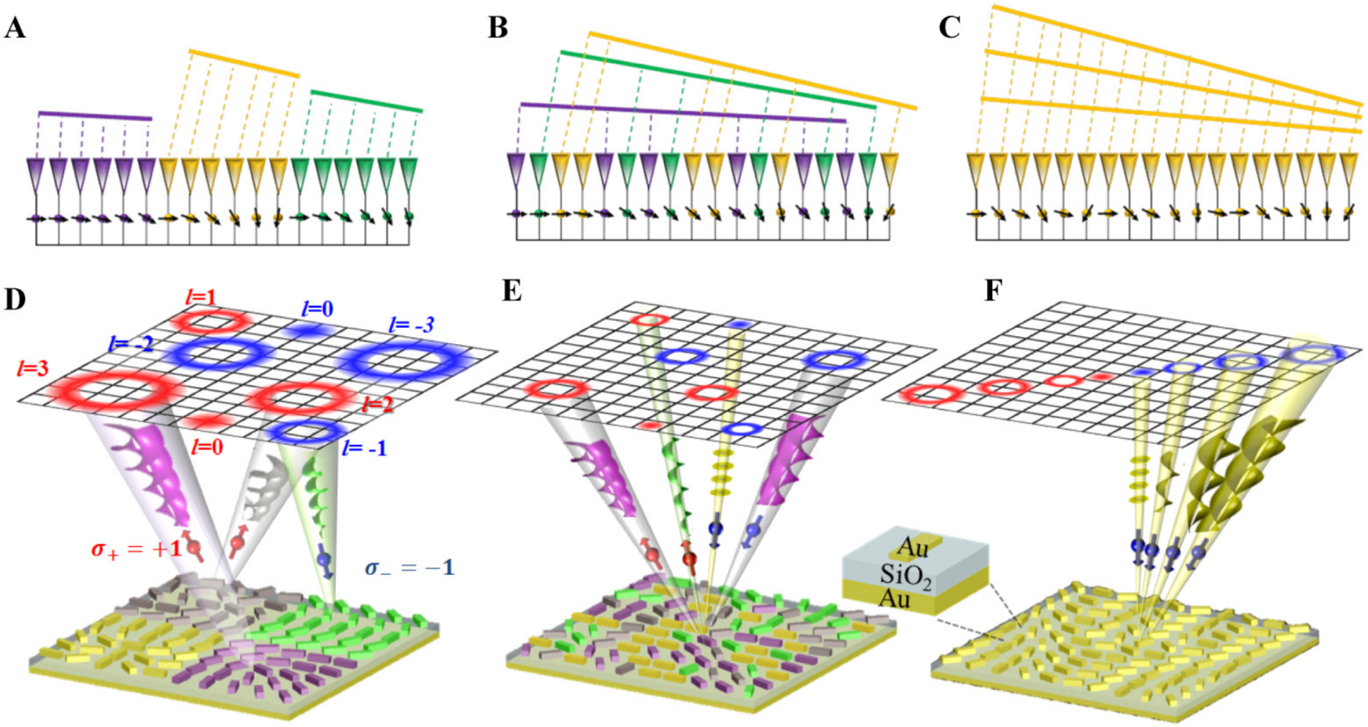

Fig. 1. Schematic of shared-aperture concepts. (**A** to **C**) Segmented (A), interleaved (B), and harmonic response (C) one-dimensional phased arrays. (**D** to **F**) Schematic far-field intensity distribution of wave-fronts with positive (red) and negative (blue) helicities emerging from segmented (D), interleaved (E), and harmonic response (F) GPMs composed of gap-plasmon nanoantennas (inset). Here *l* stands for the topological charge of the spin-dependent OAM wave-fronts [for more details see (*22*)].

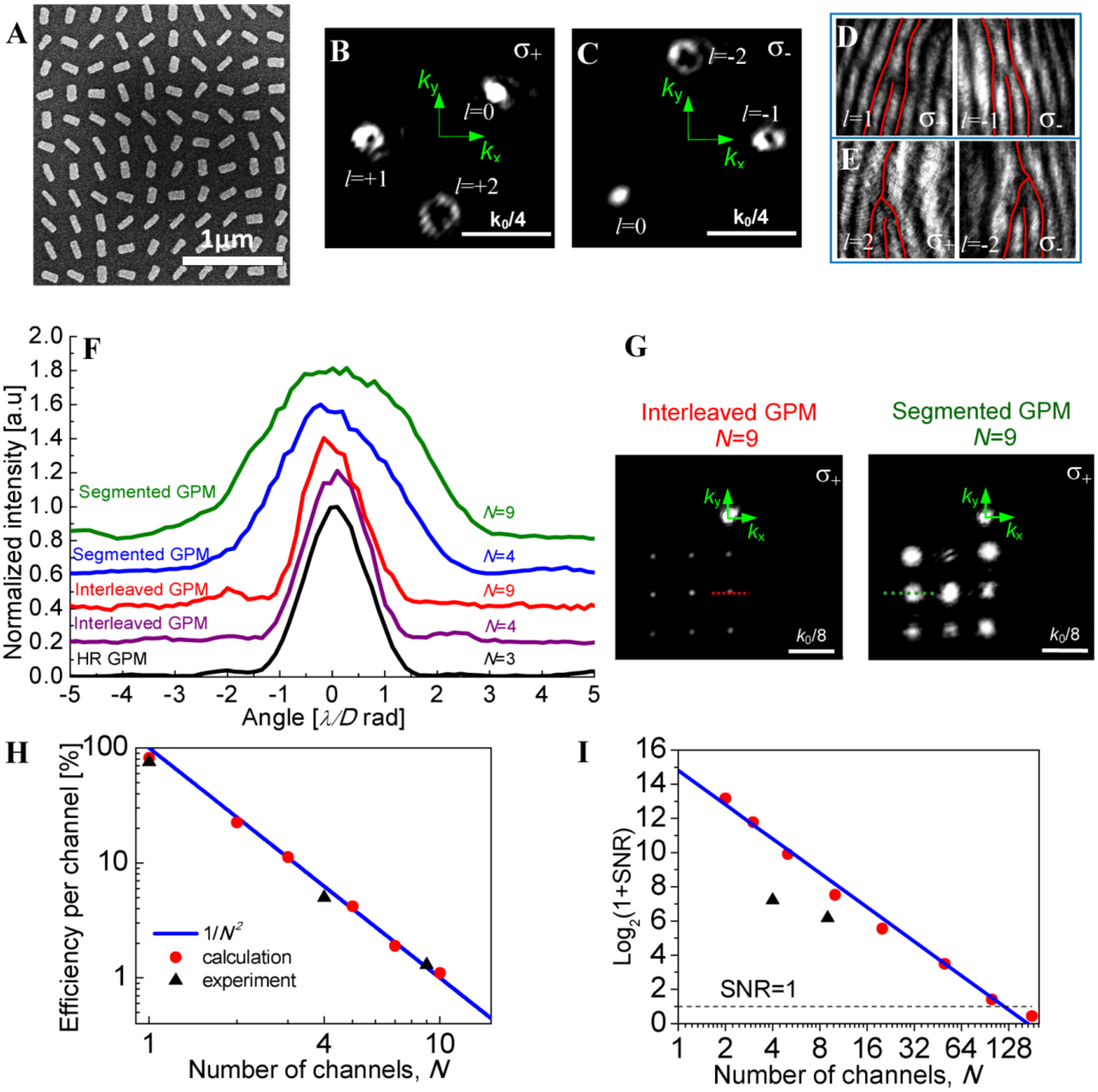

Fig. 2. Multiple wave-front shaping via interleaved GPMs. (A) Scanning electron microscope image of a gap-plasmon GPM of aperture D = 50 μm. (B and C) Measured spin-flip momentum deviation of three wave-fronts with different OAMs; $\sigma_{\pm}$ denotes the incident spin. (D and E) Interference pattern of the spin-flipped components with a plane-wave, observed from different GPMs generating OAM wave-fronts of $l = \pm 1$ (D) and $l = \pm 2$ (E), for σ_{-} and σ_{+} illumination. (F) Observed angular width of plane-waves emerging from shared-aperture GPMs of different types and numbers of generated channels, corresponding to different colors. (G) Measured momentum deviations for the interleaved and segmented GPM, wherein the intensity distributions of nine channels in (F) are presented along the dashed colored lines. (H and I) Efficiency per channel (H) and number of bits per channel (I); here red dots and black triangles denote the calculation and experiment results, respectively, whereas the blue fit corresponds to ~$1/N^2$.

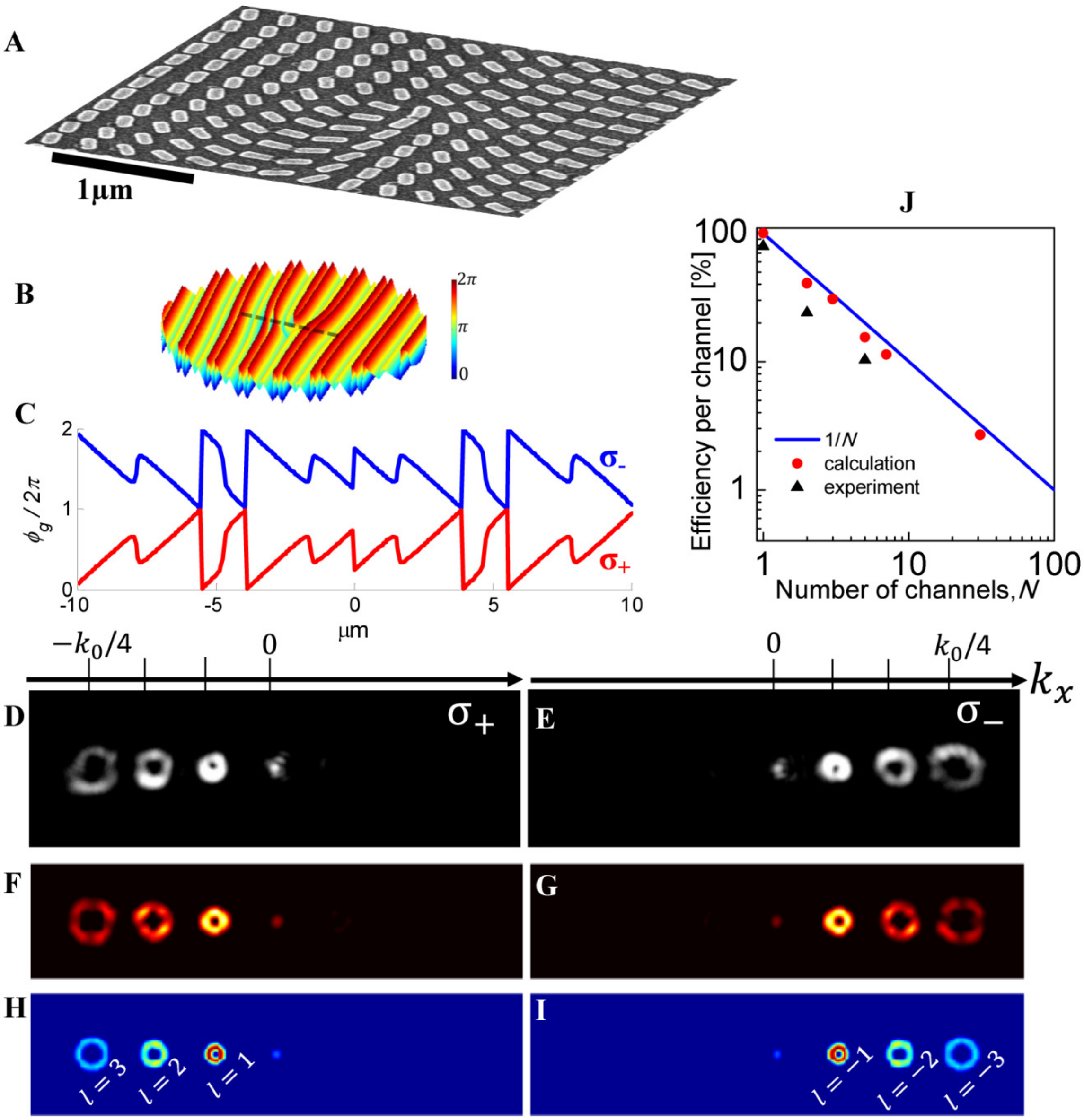

Fig. 3. Spin-dependent asymmetric harmonic response. (**A**) Scanning electron microscope image of the fabricated gap-plasmon HR-GPM. (**B**) The geometric phase distribution of the entire HR-GPM for σ_+. (**C**) The calculated phase distributions along the 20 μm dashed line in (B) for σ_- (blue) and σ_+ (red). (**D** to **I**) Measured (D and E), FDTD simulated (F and G), and calculated Fourier amplitudes (H and I) spin-dependent HR diffractions of OAM orders, for right (σ_+) and left (σ_-) circular polarization illuminations at a wavelength of $\lambda = 760$ nm, respectively. Note, the dim zero order spot arises from an additional harmonic of the "triplicator" phase function, and is of negligible efficiency of 2%. (**J**) Efficiency per channel, red dots and black triangles denote the calculation and experiment results, respectively, whereas the blue line corresponds to 1/*N*.

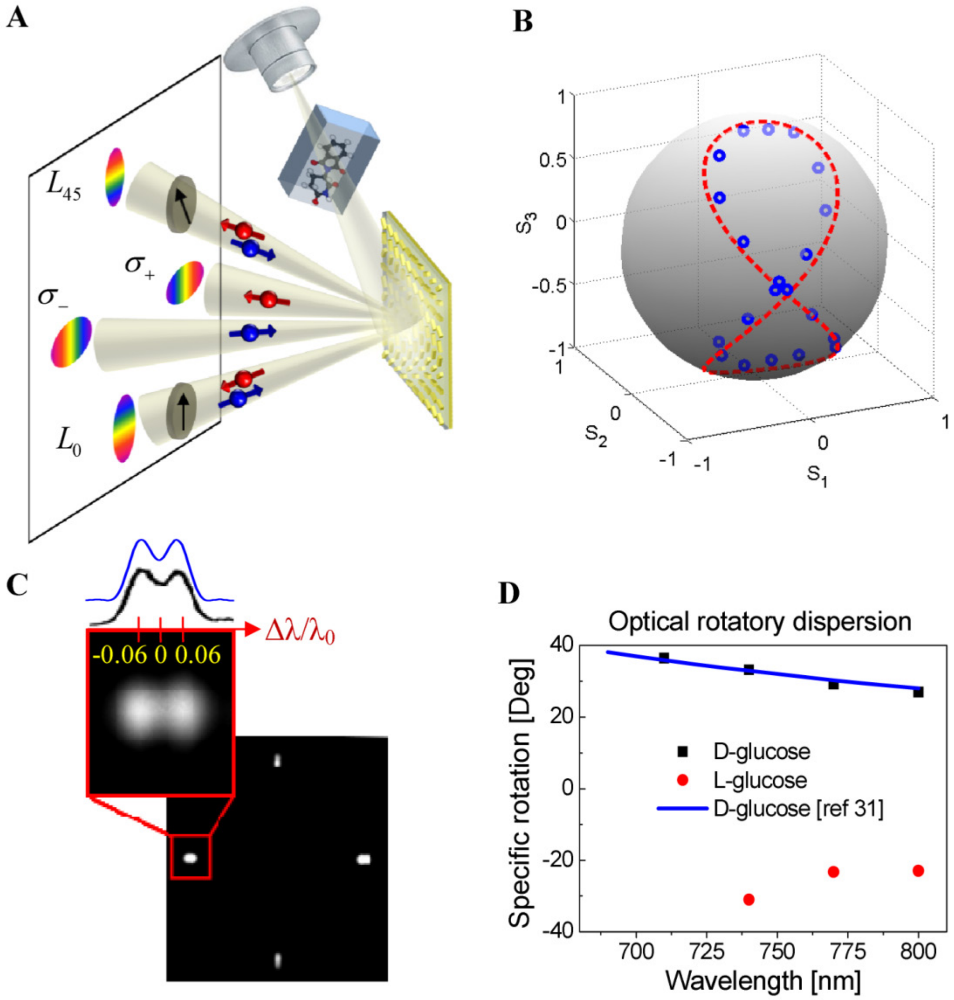

Fig. 4. Spectropolarimeter metasurface. (**A**) Schematic setup of the spectropolarimeter wherein the SPM is illuminated by a continuum light passing through a cuvette with chemical solvent; then, four beams of intensities $I_{\sigma_+}, I_{\sigma_-}, I_{L45}, I_{L0}$ are reflected toward a CCD camera. (**B**) Predicted (red dashed curve) and measured (blue circles) polarization states, obtained by a polarization-state generator (linear polarizer followed by a rotated quarter-wave plate), depicted on a Poincaré sphere. (**C**) The measured far-field intensities for elliptical polarization at two spectral lines, 740 nm and 780 nm wavelengths, and the corresponding resolving power of the SPM of 50 μm diameter (inset, black line) and calculation (blue line). (**D**) Optical rotatory dispersion for the specific rotations of D- and L-glucose. Red circles and black squares represent the measured ORD of D- and L-glucose, respectively, where the blue line depicts the dispersion acquired from (*31*).

Photonic spin-controlled multifunctional shared-aperture antenna array

Elhanan Maguid, Igor Yulevich, Dekel Veksler, Vladimir Kleiner, Mark L. Brongersma and Erez Hasman (April 21, 2016)

Science (print ISSN 0036-8075; online ISSN 1095-9203) is published weekly, except the last week in December, by the American Association for the Advancement of Science, 1200 New York Avenue NW, Washington, DC 20005.